Physica D 404 (2020) 132346

Contents lists available at ScienceDirect

Physica D

journal homepage: www.elsevier.com/locate/physd

A crisis for the verification and validation of turbulence simulations

James Glimm [a,1,*], Baolian Cheng [b,1], David H. Sharp [b,1], Tulin Kaman [c,1]

[a] Stony Brook University, Stony Brook, NY 11794, United States of America
[b] Los Alamos National Laboratory, Los Alamos, NM 87545, United States of America
[c] University of Arkansas, Fayetteville, AR 72701, United States of America

ARTICLE INFO

Article history:
Received 30 May 2019
Received in revised form 26 November 2019
Accepted 15 January 2020
Available online 24 January 2020
Communicated by V.M. Perez-Garcia

Keywords:
Turbulence
DNS
ILES
Energy dissipation rate
Admissibility
Type Ia supernova

ABSTRACT

Three algorithms have been proposed for solution of the Rayleigh–Taylor turbulent mixing problem. They are based upon three different physical principles governing the Euler equations for fluid flow. The principles serve to select the physically relevant solution from among many nonunique solutions. The admissibility principle is in dispute. The three different algorithms, expressing the three physical admissibility principles can be formulated in terms of the three energy dissipation rates or the entropy production rates, as selected by the size of the sub grid scale coefficients. These have maximal values or less than maximal values. The resulting solutions are markedly different.

We find strong validation evidence that supports the maximum rate principle, based on a review of prior results and on new results presented here. We review experimental data used for validation and sufficient to discriminate among the three. We present a new analysis of this data. We show that the hypothesized long wave length perturbations in the initial conditions are not significant, so that validation can be based on this data in a straight forward manner.

One of the algorithms is labeled direct numerical simulation, but is not, and as a consequence, the two algorithms with less than maximal SGS coefficients are variants of one another.

Recommendations for the numerical modeling of the deflagration to detonation transition in type Ia supernova are discussed.

1. The crisis for V&V

The solutions of the Euler equation for fluid dynamics are not unique. An additional physical principle in the form of an admissibility criterion is needed to select the physically meaningful solution. Wild and manifestly nonphysical solutions have been studied extensively [1,2]. These constructions offer cautionary counter examples to enlighten studies of the Euler equation as a model for fully developed turbulence. This paper is concerned with less dramatic, and in that sense more troublesome, examples of the nonuniqueness for Euler equation solutions: ones that are the limit of mesh generated solutions as the mesh tends to zero.

We identify three different algorithms with markedly different solutions, based on three different physical principles of admissibility. The primary distinction among the three is in the grid level dissipation of energy: maximal or two levels of submaximal. We find strong evidence that the dissipation of energy occurs at a maximum rate, which we formulate as a necessary admissibility condition. We introduce new evidence and review existing evidence to justify this conclusion.

The nature of the problem is summarized in the quote from [3], Section 6 from the comprehensive survey articles [3,4], regarding evaluation of the Rayleigh–Taylor (RT) instability growth rate α_b, (See Section 3 for a definition of α_b.) "agreement between simulations and experiment are worse today than it was several decades ago because of the availability of more powerful computers". The quote defines a challenge to existing standards of verification and validation (V&V). While the governing physics model is disputed, the crisis persists. The evidence presented here, supporting the principle of a maximum rate of dissipation admissibility, falls within the general framework of V&V.

Pending a resolution of the admissibility issues, the crisis remains. It pertains not to the V&V methodology, but rather to the lack of its application to this problem. This paper contributes a resolution of the V&V crisis, in favor of the maximum rate principles for admissibility.

If turbulence or non turbulent stirring is present in the problem solved, we propose that *the standards of V&V should ensure the physical relevance of the solutions obtained.*

1.1. RANS, LES and DNS

Reynolds averaged Navier–Stokes (RANS) simulations resolve all length scales needed to specify the problem geometry. Large

* Corresponding author.
E-mail addresses: glimm@ams.sunysb.edu (J. Glimm), bcheng@lanl.gov (B. Cheng), dcso@lanl.gov (D.H. Sharp), tkaman@uark.edu (T. Kaman).

[1] All authors contributed equally.

https://doi.org/10.1016/j.physd.2020.132346
0167-2789/

eddy simulations (LES) resolve not only these scales, but in addition they resolve some, but not all, of the generic turbulent flow. The mesh scale, i.e., the finest of the resolved scales, occurs within the turbulent flow. As this lies in a strongly coupled flow regime, problems occur at the mesh cutoff. Resolution of all relevant length scales, known as Direct Numerical Simulation (DNS) is computationally infeasible for many problems of scientific and technological interest.

According to ideas of Kolmogorov [5], denoted K41, the energy in a turbulent flow, conserved, is passed in a cascade from larger vortices to smaller ones. This idea leads to the scaling law

$$\langle |v(k)|^2 \rangle = C_K \epsilon^{2/3} |k|^{-5/3} \tag{1}$$

for the Fourier coefficient $v(k)$ of the velocity v. Here C_K is a numerical coefficient and ϵ, the energy dissipation rate, denotes the rate at which the energy is transferred within the cascade from the large scales to the smaller ones. It is a measure of the intensity of the turbulence.

1.2. Three models for the Reynolds stress

Grid values for numerical solutions of the Euler and Navier–Stokes equations are interpreted as cell averages. Because the equations are nonlinear, the averaging produces an error (the difference between the average of a product and the product of the average). This difference, known as the Reynolds stress,

$$\text{Reynolds Stress} = \overline{v}\,\overline{v} - \overline{vv}\ , \tag{2}$$

occurs on the right hand side (RHS) of the discretized Euler or Navier–Stokes equation. As it is a sub grid quantity, unknown at the grid level, a grid level model of the Reynolds stress is needed as an approximation. The Sub Grid Scale (SGS) terms, added to the RHS of the momentum and species concentration equations, generally have the form

$$\nabla \nu_t \nabla \quad \text{and} \quad \nabla D_t \nabla\ . \tag{3}$$

The coefficients ν_t and D_t are called viscosity and diffusivity SGS coefficients. The Reynolds stress analysis motivates the SGS coefficient ν_t, while a similar average of the equation for the transport of species concentration motivates D_t.

At the grid level, the numerically modeled cascade is broken. Energy accumulates at the grid level. In this manner, the sub grid scale flow exerts an influence on the flow at the resolved level. The SGS terms (3) serve to dissipate this excess grid level energy so that the resolved scales see grid level data as if the cascade had continued into the smaller (sub grid) scales.

The three algorithms belong to the LES family. The maximum dissipation algorithm (as measured by the size of the SGS terms) is FronTier. It is based on dynamic SGS models in the spirit of [6,7], and front tracking. A limited dissipation algorithm is Implicit Large Eddy Simulation (ILES). A variant of ILES, also with limited dissipation, claims to be DNS, but is not. We call it macro DNS (MDNS), to distinguish it from true DNS. A definition of DNS is that the mesh scale Reynolds number should be unity. In MDNS, the velocity differences occurring in the Reynolds number are not correctly evaluated. The required peak value (an L_∞ norm) for the velocity difference is replaced by the global average (an L_1 norm of velocity fluctuations). This definition is not found in the undocumented MDNS study [8], but is found in [9]. The result is a time dependent, globally constant in space SGS coefficient multiplying a simple version of the Smagorinsky model (MDNS) or a higher order version of the Smagorinsky model (ILES, MIRANDA). The resulting SGS choice and the algorithm it produces is dependent on the mesh resolution. MDNS results at varying degrees of disagreement to experiment have been obtained. The energy dissipated at the grid level is determined by the SGS coefficients in the three algorithms. In regions of intense turbulence, FT dissipates more energy than the others. In regions of low turbulent intensity, ILES and MDNS could artificially dissipate more energy. These facts are reflected in Table 4.

1.3. The three physical principles: a V&V selection

The three physical principles lead to three distinct algorithms, which differ in their treatment of mesh level dissipation of energy, from limited to full (maximum) dissipation rates. The more recent MDNS algorithm, enabled by today's large scale computers in [8], shows the largest disparity relative to experiment, providing the basis for the comment of Zhou, that large scale computers have increased the disparity between simulation and experiment.

Extensive experimental validation evidence with data from [10,11] is reviewed in summary form in Section 3. A new simulation showing comparison of scaling law exponents is also presented in Section 3. Both strongly favor the maximum dissipation rate. We quote from Zhou [3], Section 5.2, in discussing the FronTier solution [12]:

"it was clear that accurate numerical tracking to control numerical mass diffusion and accurate modeling of physical scale-breaking phenomena and surface tension were the critical steps for the simulations to agree with the experiments of Read and Smeeton and Youngs".

The data [10,11] is unique in its use differentiating among these principles. This data has been discounted due to the possibility of long wave length perturbations ("noise") in the initial data. There is no experimental basis for noise of sufficient strength. We show the opposite: its strength is insufficient to modify the turbulent mixing rate α_b appreciably. The data of [13] could in principle serve the purpose of comparison of algorithms, but it has not been simulated in comparison studies. The initial data of [13] is analyzed in [14], wherein long wave length noise is asserted to be significant. We will discuss this issue in Section 2.4.

The noise hypothesis for the [10,11] data, widely discussed in the literature, concerns initial condition noise. Noise in the form of mode 1 perturbations generated during the acceleration process is discounted as follows. Such, if lateral, side to side sloshing would generate mode 1 signals in the developing wave front. This was excluded through Plate 4 of [10,11] through an analysis of Plate 4 bubble tip noise, which produced data consistent with the Plate 3 bubble tip noise, and was shown to be negligible in its effect on α_b. Mode 1 perturbations in plates 5 and 6 (the final of the experiment) can be excluded from visual inspection. Noise in the direction of the acceleration would manifest itself in a noisy perturbation on the t^2 growth rate for α_b. There is no sign of such noise in the α_b growth rate of size sufficient to affect α_b appreciably, and it has never been postulated to occur in the [10,11] data.

On the basis of our demonstration that the noise in the data [10,11] is of minor importance in its effect on the values of the RT mixing rate α_b, we use this data directly in a validation study. We point to the extensive record of FronTier simulations (maximum rate algorithm) in agreement with the [10,11] data. This combination (simulation in agreement with noise free experimental data) is a proof of validation.

Verification in the traditional sense of convergence under mesh refinement has been addressed [15,16]. Verification related to assessing the proper admissibility law of physics will be addressed in separate publications.

The two less than maximum dissipation algorithms model the Reynolds stress with a clear departure from a maximum dissipation rate, and thus violate the postulated maximum rate of physics for fluid turbulence.

1.4. SGS terms: three choices

ILES is the computational model in which the minimum value of ν_t is chosen (minimum of grid level excess energy is removed) to retain the $|k|^{-5/3}$ scaling law. The prefactor $C_K\epsilon^{2/3}$ is not guaranteed. ILES depends on limited and globally defined SGS terms. It does not use the sub grid terms that correspond to the local values of the energy dissipation cascade. Miranda is a modern compact scheme. An ILES version of Miranda is presented in [17]. This reference provides details for the ILES construction. The sub grid terms are chosen not proportional to the Laplacian as in (3), but as higher order dissipation rates, so that small wave numbers are more strongly suppressed. The SGS modeling coefficients ν_t and D_t are chosen as global constants. The basis for the choice is to regard the Reynolds stress and the accumulation of energy at the grid level as a Gibbs phenomenon to be minimized [17]. Miranda achieves the ILES goal of an exact $-5/3$ spectral decay, see Fig. 3 right frame in Ref. [17].

FronTier uses dynamic SGS models [6,7], and additionally uses a sharp interface model to reduce numerical diffusion. In this method, SGS coefficients ν_t and D_t are defined in terms based on local flow conditions, using locally defined turbulent scaling laws, extrapolated from an analysis of the flow at one scale coarser, where the sub grid flow is known. This local scaling need not come from Kolmogorov or more advanced [18] scaling laws. FronTier allows the locally modified scaling laws that occur with weakly quasi stationary flows. The actual definition of the dynamic SGS algorithm is discussed in Section 5.3 and is based on raising the energy dissipation rate to the maximum level permitted by local flow conditions.

The MDNS algorithm is a variant of ILES, with a different, but less than maximal choice of SGS coefficients. It is not based on a physical principle but rather on the belief that MDNS is true DNS (or at least sufficiently close to true DNS) and as such, employs sufficient sub grid terms.

Through the choice of Reynolds stress modeling, the ILES and MDNS algorithms block some fraction of the locally defined grid level dissipation, as estimated by turbulent scaling laws. By energy conservation, this grid level choice blocks dissipation in the entire turbulent cascade, and results in the observed decrease in the observed values of α_b. Thus we see that the Reynolds stress is an inherently physical quantity.

Regarding the Reynolds stress as a Gibbs phenomenon, a numerical artifact, and on this basis minimizing its possible values, is the direct cause of the lower α_b values ILES achieves.

Solution differences between FronTier and ILES were reviewed in [19], with FronTier but not ILES showing agreement with the data [10,11]. The MDNS solutions [8] and choice of SGS terms are even further from experimental validation while the MDNS solutions [9] are closer to experimental α_b values, but still in disagreement with experiments.

A number of authors label simulations as DNS in which the simulation Δx is modestly larger than the Kolmogorov scale. It seems to be a universal practice in such studies, however, to include comparison to experiment relative to the quantity of interest. In other words, use of resolution coarser than true DNS is accompanied by a validation study. For [8], this standard is not followed. Moreover, the mesh size of MDNS beyond DNS is not modest.

The Refs. [20,21] focus on the local turbulent intermittency at the MDNS defined scale. These papers find a range of power law behavior which indicates that MDNS is in fact not true DNS.

1.5. A non equilibrium thermodynamics perspective

A mathematical proof of the principle of maximum entropy production was derived [22,23] from laws of statistical physics, based on the thermal fluctuations of particle positions. The use of a maximum entropy production admissibility principle is familiar from numerical modeling of shock waves. This entropy is also the thermal entropy of the molecules.

The entropy related to turbulence concerns random fluctuations of the particle velocities, rather than their positions.

The maximum rate of entropy production, as an admissibility condition for fully developed turbulence, is an extension of the second law of thermodynamics, in the sense that under this extension, a most probable (statistical expectation) path for the dynamic evolution of entropy increase is tightly constrained and usually unique. The theories of maximal rates (of energy dissipation or entropy production) have an ambiguous history. This principle has been applied successfully to many natural processes [24] including problems in climate science (terrestrial and other planets) [25], in astrophysics, and the clustering of galaxies. As noted in [26], it does not have the status of an accepted law of physics. The analysis [27] studies the principle of maximum entropy production of Ziegler [28,29] and its relation to the opposite theory of minimal entropy production by Prigogine [30].

Prigogine's analysis applies to deterministic flows, and the maximal rates apply to energy dissipation. Motivated by the analysis of [27], and for physics restricted to single density incompressible fluid flow, we observe that the acceleration (after projection onto the curl subspace of the velocity fields, to eliminate gradient pressure forces), can be divided into a sum of deterministic and dissipative parts. For descriptions of fully developed turbulence, we omit viscous diffusion forces. The deterministic part is defined by the Prigogine theory, and the dissipative part occurs at a maximum dissipation rate. For energy conserving algorithms, this division is assured, and if either is maximized, so is the other.

Momentum conservation, imposed locally in space and time, defines a solution of the Euler equation. This solution is also energy conserving if fractal or multifractal scaling laws are accepted, but it does not select among its nonunique solutions. The Ziegler–Prigogine controversy is not resolved by this discussion.

Experiment, i.e., validation, is the fundamental step for resolution of the Prigogine–Ziegler issue. We find validation support for the maximum rate solution for RT flows as the main thrust of this paper. See Sections 2, 3. We validate Ziegler and not Prigogine for the RT mixing dissipation rate with the data [10,11].

2. The initial condition noise level

This section and the following Section 3 establish our validation analysis in favor of the maximum dissipation algorithm. Here we show that the data [10,11] is free of significant initial perturbation long wave length noise, and thus can be used directly in validation.

2.1. Noise and LES vs. experiments

The validation data [10,11] is unique in its ability to differentiate among the three admissibility principles and in having been used to assess simulation models by the three. This data is in dispute due to the possible influence of long wave length noise in the initial conditions.

To account for observed discrepancies in predictions of $\alpha + b$ between predictions based on the minimum dissipation algorithm (ILES) and experimental data, it is common to add "noise"

to the physics model. As noise increases the entropy, some discrepancies between simulation and measured data are removed.

Thus initial condition noise is a central issue to select the physically relevant solution and admissibility principle from among the three.

2.2. Noise and immiscible experiments [10,11]

There are five experiments, all immiscible, of [10,11] with data sufficient to analyze both the long wave perturbations and the growth rate α_b, namely Exps. 56, 63, 104, 105 and 114. Initial perturbations were analyzed in [31]. The surface tension in Exps. 104, 105 and 114 is 1.37 mNm$^{!}$ = 1.37 e−5 g/ms^2.

The initial perturbations are reported separately at the time of Plate 1 and Plate 3. Plate 3 data is directly observed, while Plate 1 data is inferred from it, using deterministic exponentially growing perturbative analysis and deterministic single mode growth propagated backward in time. Plate 1 is basically the initial condition, and Plate 3 occurs approximately at the beginning of the t^2 growth of bubble interaction and bubble merger which characterizes the major part of the dynamics observed in [10,11].

For the purpose of comparison to a power law model for the noise spectrum, the Plate 1 data is needed. The resulting power law is not perfect, with the longest wave length (mode 1) perturbations showing variability by factors of 8, while the correlation between this mode 1 perturbation and α_b is basically zero.

For the purpose of modeling bubble growth in the regime of t^2 growth, the Plate 3 data is essential, as this is the time where all t^2 dynamic growth models first become applicable.

We consider two possible scenarios or hypotheses for the role of long wave length initial data perturbations.

H1. The noise affects all experiments, to elevate the noise-free value of α_b from its intrinsic value of $\alpha_b \sim 0.04$ to the observed values.

This possibility is excluded through the analysis [19,31] of a single experiment, Exp. 105 of [10,11]. We have shown that the noise is insufficient to restore agreement of ILES and MDNS with the data of [10,11]. It accounts for at most a 5% effect relative to the experimental data [11] used for validation. Our simulation analysis of multiple experiments, see [15,19] and references cited there, indicate that the α_b values have converged numerically,

Having excluded the systematic effect of noise, we now consider an alternate possibility.

H2. Fluctuations in the noise levels between distinct experiments explain fluctuations in the observed variation of α_b.

The mean of the five α_b values is $\overline{\alpha_b} = 0.065$, the standard deviation is $\sigma = 0.0061$ and the coefficient of variation is $\sigma/\overline{\alpha_b} = .094$. Table 1 presents experimental α_b and mode number perturbation spectral amplitudes, the latter dependent jointly on mode number and experiment. The tabulated entries, in units of cm, represent spectral amplitudes of directly observed data, as is defined in eq. (214) of [31] and the accompanying discussion. The process of direct measurement is also described in that reference. The missing entries are associated with late time coarse (large) bubbles, which exceed the Nyquist limit for Fourier analysis. We complete the table with entries 0 in those cases.

We analyze the data from Table 1 using the method of least squares [32,32]. In the terminology of that subject, the $y_j = \delta\alpha_b = \alpha_b - \overline{\alpha_b}$ are the observed variables and the entries Ω_{ij} of the matrix Ω defined in Table 1 are the design variables. The index j is an experiment number and the index i is a mode number. Least squares determines y_j as

$$y_j = b_0 + b_1 \sum_i \Omega_{ij} + \epsilon_j \,, \tag{4}$$

Table 1
Summary of long wave (modes 1–8) perturbation amplitude data (units cm) derived from analysis of Plate 3 of [10,11] for 5 immiscible experiments and corresponding α_b data.

Exp	56	63	104	105	114
α_b	0.058	0.069	0.068	0.072	0.060
Mode 1	0.058	0.087	0.040	0.011	0.019
Mode 2	0.021	0.057	0.010	0.013	0.011
Mode 3	0.011	0.037	0.028	0.020	0.015
Mode 4	0.025	0.057	0.007	0.006	0.016
Mode 5	0.020	0.025	0.014	0.017	0.011
Mode 6	0.021	0.028	0.024	0.012	0.006
Mode 7	0.027		0.007	0.008	0.024
Mode 8	0.008		0.017	0.012	0.011

with a residual ϵ_j of unexplained effects. We see that variation in initial perturbations explains 9% of the variation and the remainder, 91%, unexplained in this statistical analysis, is due to variation in the experimental parameters. The 9% effect is realized by analysis of modes 1–4 and is not improved when considering modes 1–8.

The 9% of the α_b variation explained by the modal perturbation analysis can be compared to the 5% uncertainty in α_b resulting from uncertainties in the bubble amplitudes that generated in the Ω_{ij} data. We are thus left with an assurance effect of 4% in the α_b amplitudes, and we can reject **H2.** as lacking in statistical significance; Even without this final subtraction, the statistical predictions give a small effect on the α_b values and their variation across experiments. On this basis we do not analyze the data further, with the conclusion that the noise effects on α_b are minor.

2.3. Noise [10,11] summary

We assert that initial condition noise in the [10,11] data is a minor contributor to the observed values of α_b. The basis for this assertion is

1. Excellent V&V results for multiple FronTier based simulations. These simulations have no noise added to the initial condition. This implies that initial condition noise does not have a major influence on α_b.
2. For simulations of Exp. 105 of [11], observed initial noise was added in the simulations. Very minor influence on α_b was observed [19,31].
3. Statistical analysis of the observed initial noise level as measured at the onset of the regime of t^2 growth (bubble merger) shows minor correlation between the observed values of α_b for 5 experiments and the corresponding noise levels. The null hypothesis that initial condition noise can generate an $\alpha_b \approx 0.04$ is rejected.
4. No validation (experimentally based) evidence has been offered to show that the actual noise levels in the experiments in [10,11] are of sufficient size to be important. Theoretical models with a power law behavior are postulated. These postulates are qualitative only, as there is no prediction (other than through our analysis) for the coefficient in front of the power law. In our analysis, the theory fails quantitatively. Systematic effects are minor and noise related variations in α_b are minor. Other studies only state: If the noise is large enough then the effect is significant.

Noise analysis is a central part of the validation issue. We offer three reasons based on experimental evidence to accept the α_b data of [10,11] as correct, with only minor modifications due to noise in the initial conditions. Equally important is the absence of a basis in experimental data or quantitatively justified physical theory for the opposing conjecture, that the initial condition noise is important.

Table 2
Least squares solution parameters, $\overline{\alpha_b} + b_0, b_1, ||\epsilon||_2$ and $||\epsilon||_2/\sigma$ for mode number combinations up to 1–8. The final column shows the fraction, 91%, of the α_b variation not explained by this statistical analysis. These effects are due to variation in experimental conditions.

Modes	$b_0 + \overline{\alpha_b}$	b_1	$\|\|\epsilon\|\|_2$	$\|\|\epsilon\|\|_2/\sigma$
Mode 1	0.0659	−0.0120	0.0061	1.0
Mode 1–2	0.0651	0.0092	0.0057	0.93
Mode 1–3	0.0644	0.0335	0.0056	0.92
Mode 1–4	0.0647	0.0258	0.0055	0.91
Mode 1–5	0.0647	0.0279	0.0055	0.91
Mode 1–6	0.0646	0.0318	0.0055	0.91
Mode 1–7	0.0653	0.0058	0.0055	0.91
Mode 1–8	0.0653	0.0051	0.0055	0.91

2.4. Noise in the initial data [13,14]

Dimonte [14] introduced a model based on the single mode RT bubble terminal velocity (proportional to the Froude number (Fr)) for the analysis of the Linear Electric Motor (LEM) RT data [13]. The model is driven by long wave length perturbations to the initial data augmented by combination of nearly adjacent mode number perturbations to form a collective perturbation.

Dimonte observed that the bubbles in [13] move more rapidly than is expected from single mode experiment, simulation and theory. The experimentally required value is $Fr \sim 1$. [14] states that bubble merger models [33] explain this recalibration of α_b. The balance of [14] explores an alternate explanation.

In citing simulation studies, [14] predates the accurate FT simulations, e.g. [15,31] in which the experimental values $\alpha_b \sim 0.06$ are obtained. The simulations reviewed in [14] are universally in disagreement with experiment. These simulations fail the Ziegler admissibility criteria of a maximal rate of LES energy dissipation. This failure of admissibility means that the simulations are not the physically relevant solutions, and should be accepted only to the degree that they agree with experiment (which they do not).

Ref. [14] continues with an analysis of a planar cross section of the early time interface location. To support a physics model based on the evolution of single modes or ensembles of them, the analysis of this data is conducted at the level of single bubbles, with a tip followed by a full column of light fluid.

Without entering into the details, we capture the general theme by stating that the analysis in [14] is based on the full bubble to spike or full midplane to bubble tip analysis. This is appropriate for a model which depends on the single mode growth rates. In contrast, the data analysis of [31] is based on fluctuations of bubble tips, an analysis consistent when the driving model is bubble interactions and mode coupling as in a bubble merger model [33].

The analysis [14] draws support from the bubble merger model [34], although as is noted by Dimonte, this model is defective in that the bubble diameter to height ration ratio disagrees with experiment by a factor of 3. The bubble merger model of [33] agrees with experiment in its ratio of bubble width to height a well as in its predictions of α_b. Thus it appears that the more accurate merger model [33] is not supportive of the analysis of [14].

The bubble tip analysis of noise is summarized in Sections 2.2, 2.3 for the data [10,11]. Here we reproduce that analysis for the data [14]. We identify 8 modes as significant outliers relative to their early time bubble height in the data [14] These bubble height modes have a mean of 0.02 and a STD of 0.14. The mean is approximately 4 times larger than the mean over the 5 experiments [10,11] tabulated in Table 1. We deduce that the noise levels in the two families of experiments are not comparable and are dependent on the experimental modalities. The LEM value $\alpha_b = 0.061$ is hardly different from the mean $\alpha_b = 0.065$. of the 5 experiments of [10,11]. This juxtaposition of these two numbers, an α_b virtually unchanged and even decreasing, while the noise level increases four-fold, suggests that the noise level is not the driving factor in setting α_b. The lack of correlation between α_b and the noise level is consistent with the analysis in Table 2. The difference between the two analyses lies in the underlying physics model which drives the analyses.

2.5. Noise [35] summary

All three algorithms compared here fail the Ziegler criteria of a maximum rate of energy dissipation. For this reason, corroboration to supporting experiments is an important aspect of V&V for these simulations. The FT algorithm is distinguished relative to ILES and MDNS in meeting this test. Additionally, the dynamic choice of the SGS coefficients in FT is closer to a maximum dissipation rate than the other two, and is actually maximal in a limited context (restriction on statistical observables predicted).

Thus we are left not with a clear resolution, but a physics level judgment between a model based on bubble height fluctuation and one based on single bubble motion. In this judgment, we have cited supporting evidence in the form of simulations in agreement with experiment and of consistency with fundamental thermodynamics admissibility criteria of Ziegler.

3. Validation: Instability growth rates and scaling laws

We refer to the RT unstable turbulent mixing process and characterize in summary the principal differences in the instability growth rates obtained from the three proposed principles of physics and the resulting three algorithms.

RT unstable flow is generated experimentally [10,11] by taking a tank, with light fluid above the heavy (stable to gravity), and accelerating it rapidly downwards, thereby reversing the gravitational and inertial forces. The resulting flow is unstable and a mixing layer grows on an acceleration (t^2) time scale, according to the formula

$$h_i = \alpha_i A g t^2 \tag{5}$$

describing the self-similar penetration h_i of the each of two fluids into the dominant phase of the other, Here $i = 1, 2$ denotes the heavy or light fluid, g is the reversed acceleration force, and the Atwood number $A = (\rho_1 - \rho_2)/(\rho_1 + \rho_2)$ is a buoyancy correction to g. ρ_i denotes a fluid density. It is common to refer to $2 = b$ penetrations as bubbles.

Table 3 summarizes the major code comparisons of this paper, based on the RT instability growth rate α_b. More detailed comparisons are found in [15,19,31] and references cited in these papers. An MDNS scheme, compact and higher order [8], has the smallest value α_b. ILES is larger but also below experimental values. The FronTier scheme using dynamic SGS is the largest of the three, uniquely in agreement with experiment.

We present a new comparison of the differences in the spectral scaling exponents among the three algorithm. Experiments do not provide a clear record of RT spectral scaling exponents, but from turbulence studies [36], we expect intermittency corrections, and a steeper than $-5/3$ decay. The velocity spectral properties in [8] and the ILES simulation [17] show a $-5/3$ spectral exponent.

As [8,17] employ thinly diffused initial layers separating two fluids of distinct densities, the immiscible experiments of [10,11] are the most appropriate for comparison. We note the very large growth of the interfacial mixing area, [8] Fig. 6, a phenomenon which we have also observed [37,38]. We believe this growth of interfacial area is a sign of a stirring instability, as discussed next.

Table 3
Three types of RT simulation algorithms according to the physics dissipation principle implemented and their value for α_b, compared to the data of [10,11].

Code	Energy dissipation	Solution properties	Evaluation relative to [10,11]
MDNS compact high order [8]	None	$\alpha_b \sim 0.02$	Inconsistent
Miranda ILES [17]	Limited	$\alpha_b \sim 0.03$	Inconsistent
FronTier [19,31]	Maximum	$\alpha_b \sim 0.06$	Consistent

Table 4
Turbulent and molecular values of viscosity and diffusivity (cm^2/s) for Exp. 112 of [10,11], using numerical resolution typical of RT simulations [19]. The turbulent viscosity and diffusivity are variable through space and time. We tabulate here two measures of these quantities: their spatial L_1 and L_∞ norms taken at a late time. The L_1 norm has been normalized through division by the volume of the experimental container. It is a simple average.

$\|\|\nu_{\text{turb}}\|\|_1$	$\|\|\nu_{\text{turb}}\|\|_\infty$	ν_{mol}	$\|\|D_{\text{turb}}\|\|_1$	$\|\|D_{\text{turb}}\|\|_\infty$	D_{mol}
1.8E−1	5.5E+1	1.01E−2	1.5E−1	5.7E+1	1.8E−5

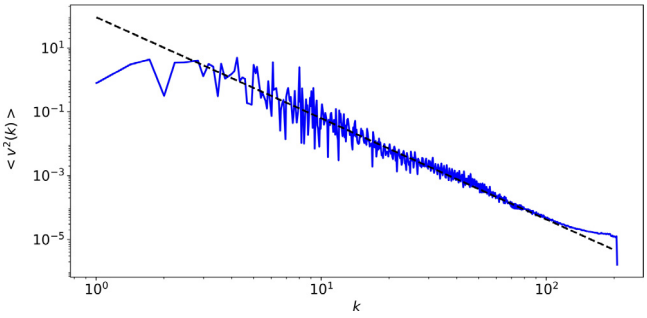

Fig. 1. Plot of the spectral decay rate, in log variables, from the two point function (as studied in [39]). Numerical data is taken from the final time step of RT simulations modeling experiment 105 reported in [19]. The immiscible decay rate −3.17 reflects a combination of turbulent intermittency and the effects of a stirring cascade.

Fig. 1, from the late time FronTier simulations reported in [19], shows a strong decay rate in the velocity spectrum, resulting from a combination of the turbulent fractal decay and a separate cascading process we refer to as stirring. Stirring is the mixing of distinct regions in a two phase flow. It occurs in the concentration equation and is driven by velocity fluctuations. For stirring, the concentration equation describes the (tracked) front between the phases. Stirring fractal behavior is less well studied than turbulent velocity. It accounts for the very steep velocity spectral decay seen in Fig. 1. MDNS and ILES [17] capture neither the expected turbulent intermittency correction to the decay rate nor any stirring correction beyond this.

4. MDNS vs. DNS

4.1. MDNS usage

True DNS of fluid flows means full resolution of all flow variables. This goal means $\eta \ll \Delta x$, with η the Kolmogorov scale and $\Delta x = 1$ the mesh spacing, for DNS relative to the viscosity, and further refinement to the Batchelor scale if the problem Schmidt number $Sc > 1$. DNS is prohibitive in computational cost, and is not achievable for most meaningful problems. The goal of DNS is to avoid the ambiguities of the SGS terms, and compute in a reliable, and model-free manner.

DNS is popular within the turbulent mixing community, with compromises involved in the usage of this term. Proponents of this use of DNS for the study of RT mixing point to possible difficulties in the experimental data, and omit experimental validation of their conclusions. In applications to RT mixing, it is believed that MDNS will give a "noise free" value for the RT mixing rate α_b relative to the data [10,11].

In essence, the compromise in the use of DNS to model RT mixing is a substitution of globally defined variables for the true DNS choice of local ones, as is explained in detail in the documentation of the DNS code, Miranda [40], in its application to RT mixing.

MDNS is analyzed in terms of global flow quantities, so that

$$Re_{\text{global}} = VL/\nu = \langle \delta v_{\text{global}} \rangle L/\nu \ , \tag{6}$$

where L is the domain length scale. V is the expectation value of the velocity fluctuations, expressed as $\langle \delta v_{\text{global}} \rangle$. The angle brackets denote a spatial ensemble average of the turbulent statistics. We estimate the unknown Δx_{DNS} in Section 4.2 from scaling laws of turbulence.

We are now in a position to define MDNS. With V as in (6), we define $Re_{\text{MDNS,mesh}} = V\Delta x/\nu$ and MDNS is defined to satisfy the equation $Re_{\text{MDNS,mesh}} = 1$, with Δx the MDNS mesh size. the value of α_b, sensitive to ν, is reduced.

In [8], pg. 563, it is stated that $\eta = \Delta x$. The assumption that η is determined from globally defined variables is clear from the context. Similarly, [8] reports a grid level Re of about 1, again using macro, not local flow parameters to define Re. Thus we conclude that [8] presents an MDNS algorithm.

The reservation is that MDNS is not true DNS, but rather is a variant of ILES, with a time dependent but globally in space constant viscous SGS coefficient for a Smagorinsky model. This solution is in itself nonunique, as it depends on the mesh resolution.

4.2. An estimate for Δx_{DNS}

Our analysis is based on (17), valid only for turbulent length scales, and omit dissipation phenomena at scales finer than the Taylor scale. The resulting estimates for the DNS mesh level Δx_{DNS} of refinement needed to achieve DNS overstate the needed refinement.

The scaling laws we need concern $\|\delta v_l\|_{L_\infty}$. This quantity is a constant relative to the turbulent statistics, so that angle brackets to average over these statistics are omitted. The quantity $\|\delta v_l\|_{L_\infty}$ represents the unresolved turbulent intensity at scale l.

We estimate the DNS mesh level Δx_{DNS} as

$$\Delta x_{\text{DNS}} = (\Delta x)^{1/10} \|\delta v_{\Delta x}/\nu\|_{L_\infty}^{-9/10} \tag{7}$$

in terms of data known at some mesh level Δx.

The global Reynolds number is defined as

$$Re_{\text{global}} = LV/\nu \ , \tag{8}$$

with L the domain size and $V = \|\delta v_{\text{global}}\|_{L_\infty}$.

We apply the scaling law (17) twice, once to determine the prefactor C and again to achieve the prediction (7).

The DNS mesh scale Reynolds number is

$$Re_{\text{DNS}} = \Delta x_{\text{DNS}} \|\delta v_{\text{DNS}}\|_{L_\infty}|/\nu = 1 \ . \tag{9}$$

The value 1 in the RHS in (9) is a commonly accepted compromise in the definition of DNS. It marks the end of the applicability of our analysis. Applying the scaling law between the global and Δx scales, we have

$$C\left(\frac{\Delta x}{L}\right)^{1/9} = \frac{\|\delta v_{\Delta x}\|_{L_\infty}}{V} \ , \tag{10}$$

which yields

$$C = \left(\frac{L}{\Delta x}\right)^{1/9} \|\delta v_{\Delta x}\|_{L_\infty}/V \ . \tag{11}$$

A similar application of the scaling law between the global and DNS scales leads to

$$C = \left(\frac{L}{\Delta x_{\text{DNS}}}\right)^{1/9} \|\delta v_{\text{DNS}}\|_{L_\infty}/V \ . \tag{12}$$

Equating the RHS of Eqs. (11), (12), we see that the global factors cancel, with the resulting identity

$$\left(\frac{\Delta x_{\text{DNS}}}{\Delta x}\right)^{1/9} = \frac{\|\delta v_{\text{DNS}}\|_{L_\infty}}{\|\delta v_{\Delta x}\|_{L_\infty}} \ . \tag{13}$$

Substituting (7) in (13), the equation

$$\left(\frac{\Delta x_{\text{DNS}}}{\Delta x}\right)^{1/9} = \left(\|\delta v_{\Delta x}/\nu\|_{L_\infty} \Delta x_{\text{DNS}}\right)^{-1} \ . \tag{14}$$

expresses Δx_{DNS} in terms of the Δx turbulent intensity and Δx mesh spacing. Solving this equation for Δx_{DNS}, we have our main result, (7).

4.3. Structure functions

The scaling laws of multifractal turbulence needed for the analysis of turbulence are described by structure functions. The structure functions give a precise meaning to clustering of bursts of turbulent intensity, compound clustering, meaning clustering of clusters etc. They measure the dependence of these compound clustering rates on the length scale of observation and thus the size of the clusters. There are two families of structure functions, one for velocity fluctuations and the other for the energy dissipation rate ϵ.

We start with a definition of the tensorial dissipation rate $\epsilon_{ij} = \nu S_{ij}^2$, with ν the kinematic viscosity and $S_{i,j} = \partial v_i/\partial x_j$ the strain rate. The scalar dissipation rate, ϵ, occurs in K41 and is recovered by the sum of $\epsilon_{i,j}$ over its tensorial indices, or more conventionally from a direct definition $\epsilon = (\nu/2)\sum_{i,j}(S_{ij} + S_{ji})^2$.

The structure functions are defined as the expectation value of the pth power of each variable. Each has an averaging radius l, which gives rise to asymptotic scaling as a power of l. For each value of p, the structure functions define a fractal related to their power law. The structure functions and the associated scaling exponents ζ_p and τ_p are defined as the expectation values

$$\langle |\delta v_l|^p \rangle \sim l^{\zeta_p} \quad \text{and} \quad \langle \epsilon_l^p \rangle \sim l^{\tau_p} \tag{15}$$

where δv_l and ϵ_l are respectively the averages of velocity differences and of ϵ. The absolute values in (15) allow non integer values of p.

In defining ζ_p we also introduce tensor indices. The i, j tensor velocity difference ζ_p is defined as $|(\delta_{+,j} + \delta_{-,j})v_i|/2$, where $\delta_{\pm,j}$ is the forward (backward) difference in the coordinate direction j with a step size l. A sum over the tensor indices i, j yields an orthogonal group invariant expression. The resulting quantity is taken to the pth power and then averaged spatially to define the i, j tensorial component of ζ_p. The definition for the scalar ϵ starts with an average over the interior of a sphere of radius l, and includes a sum over the tensor indices i, j.

The power $p = 1$ for τ_p has a special property. Assume a scaling law (15) for $\tau_{p=1}$ only and for any value of τ_1. A change in order of integration between the spatial average defining the ensemble $\langle \cdots \rangle$ and the averaging ball eliminates the average over B_l, so that the spatial average of $\epsilon(x, t)$, which we denote $\epsilon_0(t) = \int_V \epsilon(x, t)\mathrm{d}x$, is finite. It follows that $\tau_1 = 0$ and $\epsilon \in L_1(V \times [0, T])$. As is conventional in turbulence modeling, we also set the smaller p value $\tau_{1/3} = 0$.

The two families of exponents are related by a simple scaling law

$$\zeta_p = p/3 + \tau_{p/3} \tag{16}$$

derived on the basis of scaling laws and dimensional analysis by Kolmogorov [41].

Using the scaling (16), $\tau_{p/3} = 0$, and the scaling exponent is $\zeta_p = p/3$ for all p as a consequence of K41. As corrections to K41 scaling, $\tau_p = 0$ for all $p \le 3$, and $\tau_p = -2p/3 + 2 + o(1)$ according to [18]. By (16), it follows that $\zeta_p = p/9 + 2 + o(1)$ as $p \to \infty$.

The L_p norm of δv_l is $(\langle\langle(\delta v_l)^p\rangle\rangle)^{1/p}$. Substituting the τ structure function analysis of [18] into (16), we postulate that the δv_l structure functions are a mixture of exponentials, while in the large p limit, the width of the mixture of exponentials is vanishing. The scaling exponents for the L_p norms are divided by p, so that the L_∞ norm has a scaling $1/9 + o(1/p)$. In this case, the large p limit is well modeled by a single exponential, 1/9, and its prefactor, which is denoted by here C. We summarize this discussion in the formula

$$\|\delta v_l\|_{L_\infty} \sim l^{1/9} \ . \tag{17}$$

4.4. When does MDNS give correct answers?

Validation experimental data for RT other than [10,11] either do not distinguish among the alternate physical principles of admissibility conditions or have not been considered by the three algorithms.

To illustrate both of these possibilities, the hot–cold water channel experiments of [42] match simulation data for α_b for all three algorithms, and thus do not distinguish among the three physical principles. The more demanding salt-fresh water channel, which likely would have differentiated among them, was not considered in a validation study of the zero or minimum dissipation algorithms. The analogous salt-fresh water experiment Exp. 112 of [10,11], with exceedingly tight experimental error bars, provided validation data for simulations [43] of the maximum energy dissipation algorithm and physical principle. For problems which are (a) intrinsically noisy, (b) diffusive, (c) weakly turbulent, (d) limited in the objective functions used for data comparison, ILES and even MDNS algorithms can model α_b correctly [42,44].

5. Maximum dissipation rate: Verification

5.1. Energy conservation

We observe that

$$\epsilon_{V\times[0,T]} = \int_0^T \int_V \epsilon(x, t)\mathrm{d}x\mathrm{d}t < \infty \ . \tag{18}$$

and so $\epsilon(x, t) \in L_1(V \times [0, T])$ for flow in a periodic domain V, for a bounded time interval $[0, T]$, using a change of variables as outlined in Section 4.3.

An integration by parts evaluates the above integral as

$$\int_0^T \int_V \epsilon(x, t)\mathrm{d}x\mathrm{d}t = \nu \int_{V\times[0,T]} v(x, t)\Delta v(x, t)\mathrm{d}x\mathrm{d}t \tag{19}$$

as the amount of energy that has been dissipated viscously into heat. Here Δ is the Laplace operator. Due to the principle of conservation of energy, more energy cannot be dissipated into the turbulent cascade than is removed by viscous dissipation at the end of the cascade. Thus the globally averaged ϵ is a solution specific maximum dissipation value and the upper bound in (18) is justified. We remark that in the Euler limit, with zero viscosity, (19) is interpreted as saying that this dissipation occurs at distance scale 0.

We now assert that $\epsilon(x, t)$ is locally a solution specific maximum energy dissipation rate. For this purpose we assume the existence of a locally defined maximum dissipation rate, which

we call $MD(x,t)$. As $0 \le \epsilon(x,t) \le MD(x,t)$, and as its integral is the global maximum dissipation rate, the integral of the difference $MD(x,t) - \epsilon(x,t)$ satisfies

$$0 \le \int_0^T \int_V (MD(x,t) - \epsilon(x,t))\mathrm{d}x\mathrm{d}t = 0\ , \tag{20}$$

and the nonnegative integrand must vanish a.e.

The solution specific analysis does not address a comparison of the dissipation rates among multiple nonunique solutions of the Euler equation.

5.2. Weak quasi stationarity

The central verification issue here is to confirm that the dynamic SGS choice of turbulent coefficients agrees with the solution specific locally defined maximum dissipation rate $\epsilon(x,t)$. Our reasoning depends on turbulent scaling laws, and in view of the comments [36] regarding scaling laws for non stationary turbulence, we consider the weak quasi stationary hypothesis, in which scaling laws continue to hold, but with modified scaling exponents ζ_p and τ_p defined locally in space and time. The weak quasi stationary hypothesis applies to many flows of scientific and technological interest; we address later its validation for RT mixing, where it is also generally accepted.

Classical single fluid turbulence, when considered locally, is non stationary and non homogeneous. These properties refer to global aspects of turbulent flow, but they do not describe its local properties, which are far from uniform. The intermittency of clusters of turbulent intensity implies that the scaling laws when applied to local flow regions, must necessarily invoke the weak quasi stationary hypothesis.

5.3. SGS terms as models for Reynolds stress

The Reynolds stress is the basis for the three alternative constructions of the SGS terms. The Reynolds stress is the unique term in the discretized equations to involve sub grid scales. Due to its nonlinearity, it couples the resolved scales to the sub grid scales. According to turbulent scaling laws ideas, we ignore backscatter and assume that locally the Reynolds stress is identical to the energy transferred from the grid scale to the sub grid.

We coarsen the mesh by a factor of two. Then the Reynolds stress is computable and it is identical to the grid coarsened local energy dissipation rate $\epsilon(x,t)$. We recognize the Reynolds stress as a velocity difference at scale $l = \Delta x$, with turbulent scaling laws given by ζ_p, $p = 2$. Scaling for ζ_p is related to a turbulent scaling law for $\tau_{p/3}$ by (15). Scaling laws for $\langle u \Delta u \rangle$, introduced as a model for the dynamic SGS term (multiplied by u) come from τ_p, $p = 2$. From this analysis, we determine uniquely the dynamically defined SGS [6,7] turbulent coefficient ν_t, scaled from the coarsened mesh level to the current mesh level. Similar reasoning applies to the selection of the eddy diffusivity D_t, for which details are omitted.

This is not how the SGS terms are defined. At the test filter level, the known values for the Reynolds stress and the Smagorinsky model for it are known. Using these locally defined values, the required SGS coefficients are also determined at the test filter level. They are expressed as a ratio of Reynolds stress to Smagorinsky model values. Tensor degrees of freedom are suppressed in this analysis, so that the ratio is one of two scalar quantities. The key assumption in the derivation of the dynamic SGS model is that these coefficients are unchanged, and can be used at the filter level. This assumption gives rise to a cancellation, known as Germano's identity [45] and allows evaluation of the ν_t with a single level of mesh coarsening.

This description is overly simplified in two respects. It is possible to obtain negative values for ν_t. To ensure a numerically stable simulation algorithm, the ν_t is restricted to be nonnegative.

A further, and important compromise with the strict logic is the reduction of tensor components to a single scalar using least squares. In a study to be reported separately, we find that the tensor product analysis is equivalent to a restriction of the dynamic SGS method accuracy to observable quantities which are orthogonally invariant. This restriction in accuracy is reflected in the known problems in applying the dynamic SGS algorithm to turbulent boundary layers, where orthogonal invariance fails. The important RT observables, α_b and Θ are orthogonal invariant, and from this fact we have confirmation in the FT accuracy of the predictions of these observables.

These features are justified ultimately by the nearly 3 decades of validation success in the design and optimization of structures that interact with turbulent flows in real world applications.

In summary, FronTier, based on the maximum dissipation principle, models the Reynolds stress according to locally defined (weak quasi-stationary) turbulent scaling laws. The minimum dissipation algorithm, ILES, sees the Reynolds stress as a Gibbs phenomenon, and selects a minimizing model. MDNS models the Reynolds stress as zero. MDNS uses a mesh scale dependent model for these SGS coefficients, larger or smaller than ILES.

This choice of dissipation rates, applied at the mesh level only, affects the entire solution, and defines the difference among the three algorithms.

5.4. RT mixing

RT mixing is more complicated than classical turbulence. There are no externally defined stirring forces, but there are dynamically defined inertial forces. The RT inertial force is part of the RT dynamics and cannot be specified in advance.

The reduced dissipation solutions are also solutions of the Euler equation. Due to energy conservation, there is a reduction in the dynamically generated inertial forces to compensate for the Prigogine required reduction in dissipation forces. This translates into the commonly noted reduction in α_b.

The proof that the RT $\epsilon(x,t)$ is the local maximum dissipation rate proceeds as before. We consider RT mixing as two-fluid incompressible flow. The upper boundary is now reflecting, rather than periodic. We restrict the times so that each phase has not yet reached its opposite (top/bottom) wall. In this case the boundary conditions, defined by reflection symmetry, are not affected by density dependence in the gravitational or inertial forces. In reasoning regarding total energy as a finite upper bound, we include potential as well as kinetic energy, and make the same hypotheses. The proof is unchanged.

Our already noted validation for RT mixing is a validation for the weak quasi stationary hypothesis of turbulent scaling and also for the allowance to be made for the approximations with this strategy in the use of the dynamic SGS algorithm.

In selecting the maximum dissipation rate as the admissibility principle for solutions of the Euler equation, we have contributed to the resolution of the controversy between the minimum dissipation rate ideas of Prigogine and the maximum dissipation rate ideas of Ziegler, in favor of Ziegler.

5.5. Energy vs. viscous dissipation in RT simulations

We examine the FronTier simulation of Exp. 112 of [10,11]. Its dynamic SGS terms, from a late time step, give the turbulent (eddy) energy dissipation and the turbulent concentration diffusion. The SGS coefficients are variable in space and time. They are tabulated in Table 4 terms of their L_1 and L_∞ norms in space.

The SGS coefficients depend on the level of mesh resolution, with the mesh resolution $144 \times 24 \times 178$ cells used here. The molecular coefficients are small relative to their SGS counterparts. The L_1 norm of the SGS coefficient ν_t is $20\times$ larger than the molecular values and the L_∞ norm is 5000 times larger. The SGS diffusion coefficients are even larger in comparison to the molecular coefficients. indicating the dominant role of the SGS coefficients relative to the molecular coefficients. Thus molecular coefficients can be neglected in an approximate analysis.

6. Significance: An example

For highly complex physical processes, domain knowledge must be retained. It appears to be more feasible to bring multifractal modeling ideas into the domain science communities than the reverse. In this spirit, we propose here a simple method for the identification of (turbulence related) extreme events through a modification of adaptive mesh refinement (AMR), which we call Fractal Mesh Refinement (FMR). We propose FMR to seek a deflagration to detonation transition (DDT) in type Ia supernova.

AMR refines the mesh wherever the algorithm detects under resolution. In contrast, FMR skips over most of these under resolved refinements, and only refines in those extreme cases of under resolution which are potential candidates for DDT. By being more selective in its refinement, FMR allows high levels of strongly focused resolution, a feature which enhances the chance of discovery of highly concentrated deflagration fronts as a precursor to DDT. The method is thus proposed to assess as possible preconditions for a DDT the extreme events generated by multifractal turbulent nuclear deflagration. Such events, in a white dwarf type Ia supernova progenitor, are assumed to lead to DDT, which produces the observed type Ia supernova. See [46,47] and references cited there.

The detailed mechanism for DDT is presumed to be diffused radiative energy arising from some local combustion event of extreme intensity, in the form of a convoluted flame front, embedded in a nearby volume of unburnt stellar material close to ignition. Consistent with the Zeldovich theory [48], a wide spread ignition and explosion may result. FMR refinement criteria will search for such events. See [49] for a more detailed development of these ideas. In [50], initial conditions with a high local concentration of deflagration fronts are shown to lead to a DDT.

There is a minimum length scale for wrinkling of a turbulent combustion front, called the Gibson scale. Mixing can proceed in the absence of turbulence via stirring. Thus the Gibson scale is not the correct limiting scale for a DDT event. Stirring, for a flame front, terminates at a smaller scale, the width of the flame itself. The analysis of length scales must also include correctly modeled transport for charged ions [51], which can be orders of magnitude larger than those inferred from hydro considerations. The micro structure of mixing for a flame front could be thin flame regions surrounded by larger regions of burned and unburned stellar material (as with a foam of soap bubbles, with a soap film between the bubbles). Here again multifractal and entropy issues appear to be relevant. A multifractal clustering of smaller bubbles separated by flame fronts can be anticipated, and where a sufficient fraction of these bubbles are unburnt stellar material, a trigger for DDT could occur.

This micro structure is a further law of physics, and for flame fronts, the change of topology of the flame front occurs more frequently than would occur in a pure stirring scenario.

For implementation of the above analysis, the astrophysics code should be based on dynamic SGS, not on ILES.

7. Conclusions

The main result of this paper is the selection of the maximum rate admissibility principle to complete the otherwise under specified Euler equations, and in application to RT, to accept the maximally dissipative algorithm as physically correct.

Validation. Validation for RT simulations is the heart of this paper. We itemize the three key steps:

1. Identification of the data [10,11] as uniquely distinguishing among the three admissibility principles and in having been tested for all three.
2. Absence of significant noise in this data, so that it can be used for validation purposes.
3. Extensive numerical simulation based on the maximum rate principle, and in agreement with the [10,11] data.

Verification. With input from the validation step, the weakly quasi stationary hypothesis for the RT data allows the use of turbulent scaling laws for non stationary flows.

A detailed justification of the dynamic SGS method as maximizing the energy dissipation rate as measured by orthogonally invariant observables will be presented separately.

The quasi stationary hypothesis is generally accepted for RT flows and many other non stationary flows and will be the subject of a further, and separate, analysis. This hypothesis is consistent with the dynamic SGS terms used in the FronTier code, so that the validation step includes validation of this hypothesis for RT. With the RT validation as a physics input, the mathematical verification of the statistical analysis proceeds through identification of the Reynolds stress with the dynamic SGS model for it.

Relevance. We have contributed to the resolution of the Prigogine–Ziegler controversy regarding energy dissipation rates of turbulent flow, in favor of the maximum dissipation rate of Ziegler.

We have noted the potential for ILES related errors to influence ongoing scientific investigations, including the search for DDT in type Ia supernova.

Outlook. V&V standards should include an analysis of the physical relevance of proposed solutions to problems which include turbulent or stirring phenomena.

We recognize that the conclusions of this paper will be controversial within the ILES and high order compact turbulent simulation communities.

A deeper consideration of the issues raised here is a possible outcome. The issues to be analyzed are clear:

- Is there an experimental (validation) basis for asserting that sufficient noise is present in the [10,11] data? Is there some other data set which will distinguish between the three admissibility principles?
- Is the transport of energy and concentration limited at the grid level in ILES and its variant MDNS, correct physics? Are the full standards of DNS simulations to be ignored in simulations claiming to be DNS? If MDNS is used, is there a need for a separate validation step?
- Is the energy dissipation and the Reynolds stress to be regarded as a Gibbs phenomenon [17], and thus to be minimized?
- Should a solution using established algorithms and in full satisfaction of standards of V&V be accepted as correct?

A response to the V&V issues raised here by appeal to consensus (everyone else is doing it) necessarily fails. Consensus violates standards of V&V, and for this reason it is a weak argument. The engineering community using dynamic SGS models is far larger than the community of ILES users. Dynamic SGS models are used in the design of engineering structures and in the calibration

of RANS models. They are backed by nearly three decades of extensive experimental validation and experience in the design and optimization of engineering structures tested in real applications. Consensus in this larger community overwhelms the ILES consensus by its magnitude and by its nearly three decades of designed structures that are "use tested" in actual operations. ILES loses the consensus argument.

Acknowledgments

Use of computational support by the Swiss National Supercomputing Centre is gratefully acknowledged. We thank Perry Johnson for helpful comments. Los Alamos National Laboratory Preprint LA-UR-19-20285. Helpful comments from the referees are acknowledged.

References

[1] C. De Leliss, L. Szekelyhidi, Ann. of Math. 170 (2009) 1471.
[2] C. De Leliss, L. Szekelyhidi, Arch. Ration. Mech. Anal. 195 (2010) 225.
[3] Y. Zhou, Phys. Rep. 720–722 (2017a) 1, http://dx.doi.org/10.1016/j.physrep.2017.07.005.
[4] Y. Zhou, Phys. Rep. 723–725 (2017b) 1, http://dx.doi.org/10.1016/j.physrep.2017.07.008.
[5] A.N. Kolmogorov, Dokl. Akad. Nauk SSSR 30 (1941) 299.
[6] M. Germano, U. Piomelli, P. Moin, W.H. Cabot, Phys. Fluids A 3 (1991) 1760.
[7] P. Moin, K. Squires, W. Cabot, S. Lee, Phys. Fluids A 3 (1991) 2746.
[8] W. Cabot, A. Cook, Nat. Phys. 2 (2006) 562.
[9] D. Livescu, T. Wei, M.R. Petersen, J. Phys. Conf. Ser. 318 (2011).
[10] K.D. Burrows, V.S. Smeeton, D.L. Youngs, AWE Report Number 0 22/84, 1984.
[11] V.S. Smeeton, D.L. Youngs, AWE Report Number 0 35/87, 1987.
[12] E. George, J. Glimm, X.-L. Li, Y.-H. Li, X.-F. Liu, Phys. Rev. E 73 (2006) 016304.
[13] G. Dimonte, M. Schneider, Phys. Rev. E 54 (1996) 3740.
[14] G. Dimonte, Phys. Rev. E 69 (2004) 056305.
[15] H. Lim, J. Iwerks, J. Glimm, D.H. Sharp, Proc. Natl. Acad. Sci. 107 (29) (2010a) 12786, Stony Brook University Preprint SUNYSB-AMS-09-05 and Los Alamos National Laboratory Preprint LA-UR 09-06333.
[16] H. Lim, J. Iwerks, Y. Yu, J. Glimm, D.H. Sharp, Phys. Scr. T142 (2010b) 014014, Stony Brook University Preprint SUNYSB-AMS-09-07 and Los Alamos National Laboratory Preprint LA-UR 09-07240.
[17] B.E. Morgan, B.J. Olson, J.E. White, J.A. McFarland, J. Turbul. 18 (2017).
[18] Z.S. She, E. Leveque, Phys. Rev. Lett. 72 (1994) 336.
[19] H. Zhang, T. Kaman, D. She, B. Cheng, J. Glimm, D.H. Sharp, Pure Appl. Math. Q. 14 (2018) 193, los Alamos National Laboratory preprint LA-UR-18-22134.
[20] Y. Kandea, K. Morishita, J. Phys. Soc. Japan 7 (2007).
[21] B. Sawford, P.K. Yeung, 27, 2015.
[22] O. Lanford, Lecture Notes Phys. 20 (1973).
[23] J.L. Lebowitz, Prog. Theor. Phys. suppl. 20 (1978).
[24] L.M. Martyushev, V.D. Seleznev, Phy. Rep. 426 (2006) 1.
[25] H. Ozawa, A. Ohmura, R. Lorentz, T. Pujol, Rev. Geophys. 41 (2003).
[26] A. Kleidon, J. Dyke (Eds.), What is maximum entrpy productionn and how should we apply it, Entropy 12 (2010) special issue.
[27] M. Mihelich, D. Faranda, D. Pailard, B. Dubrulle, Entropy 19 (2017).
[28] H. Ziegler, in: I.N. Sneddon, R. Hill (Eds.), Progress in Solid Mechanics, Norht-Holland Publishing, Amsterdam, 1963, p. 93.
[29] H. Ziegler, C. Wehrli, Adv. Appl. Mech. 25 (1987) 183.
[30] I. Prigogine, Science 201 (1978) 777.
[31] J. Glimm, D.H. Sharp, T. Kaman, H. Lim, Phil. Trans. R. Soc. A 371 (2013) 20120183, Los Alamos National Laboratory Preprint LA-UR 11-00423 and Stony Brook University Preprint SUNYSB-AMS-11-01.
[32] D. Freedman, Statistical Models, Theory and Practice, Cambridge University Press, Cambridge, 2009.
[33] B. Cheng, J. Glimm, D.H. Sharp, Chaos 12 (2002) 267.
[34] D. Shvarts, U. Alon, D. Ofer, R.L. McCrory, C.P. Verdon, Phys. Plasmas 2 (1995) 2465.
[35] G. Dimonte, M. Schneider, Phys. Fluids 12 (2000) 304.
[36] U. Frisch, Turbulence: The Legacy of A.N. Kolmogorov, Cambridge Univeristy Press, Cambridge, 1996.
[37] H. Lee, H. Jin, Y. Yu, J. Glimm, Phys. Fluids 20 (2008) 1, Stony Brook University Preprint SUNYSB-AMS-07-03.
[38] H. Lim, Y. Yu, H. Jin, D. Kim, H. Lee, J. Glimm, X.-L. Li, D.H. Sharp, Comput. Methods Appl. Mech. Engrg. 197 (2008) 3435, Stony Brook University Preprint SUNYSB-AMS-07-05.
[39] V. Mahadeo, (Ph.D. thesis), Stony Brook University, 2017.
[40] T. Rehagen, J. Greenough, B. Olson, J. Fluids Eng. 139 (2017).
[41] A.N. Kolmogorov, J. Fluid Mech. 13 (1962) 82.
[42] N. Mueschke, O. Schilling, Phys. Fluids 21 (2009) 1, 014106.
[43] H. Lim, T. Kaman, Y. Yu, V. Mahadeo, Y. Xu, H. Zhang, J. Glimm, S. Dutta, D.H. Sharp, B. Plohr, Acta Math. Sci. 32 (2012) 237, Stony Brook University Preprint SUNYSB-AMS-11-07 and Los Alamos National Laboratory Preprint LA-UR 11-05862.
[44] N.J. Mueschke, (Ph.D. thesis), Texas A and M University, 2008.
[45] M. Germano, Tech. Rep. 116, Center for Turbulence Research, Stanford University and NASA–Ames Research Center, 1990.
[46] M. Zingale, A.S. Almgren, M.G.B. Sazo, V.E. Beckner, J.B. Bell, B. Friesen, A.M. Jacobs, M. Katz, C.M. Malone, A.J. Nonaka, et al., 2017, ArXiv:1771-06203.
[47] A. Calder, B. Krueger, A. Jackson, D. Townsley, E. Brown, F. Times, 2012, ArXiv:1205-0966.
[48] J. Lee, The Detonation Phenomena, Cambridge University Press, 2008.
[49] J. Glimm, 1806, 2018, 06054, ArXiv:1205-0966.
[50] Seitenzhal, ArXiv 2018.
[51] J. Melvin, H. Lim, V. Rana, B. Cheng, J. Glimm, D.H. Sharp, D.C. Wilson, Phys. Plasmas 22 (2015) 022708.